Electron. Mater. Lett., Vol. 13, No. 6 (2017), pp. 497-504
DOI: 10.1007/s13391-017-6390-4

Study of the Morphological, Optical, Structural and Photoelectrochemical Properties of TiO_2 Nanorods Grown with Various Precursor Concentrations

Hayoung Choi[1], Hyukhyun Ryu[1,*], and Won-Jae Lee[2]

[1]Department of Nano Science and Engineering, High Safety Vehicle Core Technology Research Center, Inje University, Gimhae 50834, Korea
[2]Department of Materials and Components Engineering, Dong-Eui University, Busan 47340, Korea

(received date: 2 December 2016 / accepted date: 28 March 2017 / published date: 10 November 2017)

Vertically aligned TiO_2 nanorods were grown on a fluorine-doped tin oxide (FTO) substrate covered with a TiO_2 buffer layer by using the hydrothermal method with various titanium precursor concentrations. In this study, the effects of the precursor concentration on the morphological, structural, optical and photoelectrochemical properties of TiO_2 nanorods were investigated. We observed that photoelectrochemical properties were mainly dependent on the nanorod length, surface area, transmittance and (002) XRD peak intensity, which indicates the oriented growth of the TiO_2 nanorods perpendicular to the substrate. As a result, the sample grown from a 0.09 M precursor solution, which grew vertically and had the highest surface area, showed the highest photocurrent density, 0.733 mA/cm^2 (at 1.0 V vs. SCE). Field emission scanning electron microscopy (FE-SEM) and atomic force microscopy (AFM) were used to characterize the morphology of the nanorods, X-ray diffraction (XRD) was used to detect the structural properties of the nanorods, UV-visual spectroscopy was used to measure the optical properties, and analysis with a three-electrode potentiostat was used to measure the photoelectrochemical properties.

Keywords: titanium dioxide, hydrothermal method, nanostructure, photoelectrochemical (PEC), photocurrent density, precursor concentration

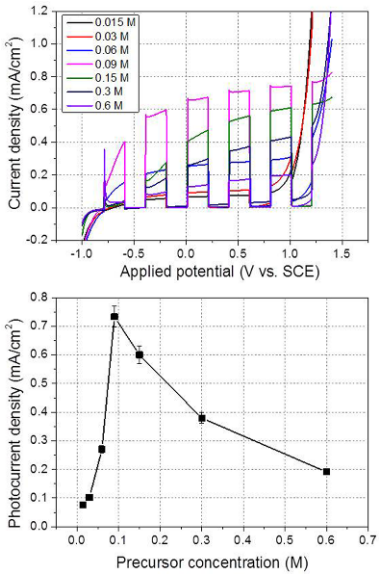

1. INTRODUCTION

Currently, studies on new, renewable energy sources are being actively conducted.[1-3] The importance of renewable energy technologies, which convert energy in the form of sunlight, wind, rain, tides, waves and geothermal to a more usable form for the consumer, is increasing due to the limited amount of fossil fuels and the environmental problems associated with their use. Hydrogen gas has garnered great interest as a candidate for a new energy source.[4,5] When hydrogen gas burns, pollution is rarely emitted, except for nitrogen dioxide and nitrogen monoxide. Hydrogen gas can be stored in various forms and does not degrade in storage. Therefore, direct solar energy-to-hydrogen energy conversion using photoelectrochemical (PEC) water splitting has received considerable attention.[6-8] An ideal semiconductor band gap for a PEC cell is larger than the theoretical minimum value of 1.23 eV needed for water splitting.[9] Semiconductors such as titanium dioxide (TiO_2), zinc oxide (ZnO), iron (III) oxide (Fe_2O_3), tungsten trioxide (WO_3) and copper (I) oxide (Cu_2O) have been investigated as photoelectrode candidates. Among these compounds, TiO_2, having an energy band gap of 3.0-3.2 eV, has many advantages, such as a very high resistance to photocorrosion; abundant reserves; nontoxicity; and insolubility in aqueous solutions, acids, alkaline solutions, and photolyzed organics. One-dimensional (1-D) TiO_2 nanostructures have an especially low recombination rate of

*Corresponding author: hhryu@inje.ac.kr

electrons and holes along with fast charge transport. Although many studies for photoelectrode using 1-D TiO_2 have been conducted since the photoelectrochemical (PEC) cell was first discovered by Fujishima and Honda in 1972, research on the optimization of 1-D TiO_2 photoelectrode is still insufficient.[10-12] The growth of 1-D TiO_2 nanostructures has been studied using various growth methods, including chemical bath deposition (CBD),[13] thermal oxidation,[14] chemical vapor deposition,[15] and the hydrothermal method.[16-18] Among these methods, the hydrothermal method is well-suited for preparing the photoelectrode, due to its many advantages such as being a low-temperature process, forming a uniform crystal phase, simplicity and high deposition rate.[19-25] Since the precursor concentration in the hydrothermal synthesis method is known to significantly affect the morphological, optical and structural properties of TiO_2 nanorods,[26,27] those properties of vertically aligned TiO_2 nanorods grown using the hydrothermal method has been widely studied.[28-31] However, there are few systematic studies reporting the mutual correlation of the properties mentioned above and the photoelectrochemical properties of TiO_2 nanorods. In this study, we investigated the effects of various precursor concentrations on the morphological, structural, and optical properties of TiO_2 nanorods, and we systematically studied the effects of these properties on the photoelectrochemical property of TiO_2 nanorods. Field emission scanning electron microscopy (FE-SEM) and atomic force microscopy (AFM) were used to characterize the morphology of the nanorods, X-ray diffraction (XRD) was used to detect the structural properties of the nanorods, UV-visual spectroscopy was used to measure the optical properties, and analysis with a three-electrode potentiostat was used to measure the photoelectrochemical properties. For the photoelectrochemical measurement, the substrate covered with the oriented TiO_2 nanorod grown from various titanium precursor concentrations was used as the working electrode, graphite was used as the counter electrode, and a saturated calomel electrode (SCE) was used as the standard electrode.

2. EXPERIMENTAL PROCEDURE

Fluorine-doped tin oxide (FTO) substrates were sonicated in acetone and methanol for 10 min each, rinsed in distilled water and dried in filtered air. Then, the substrates were dried at 60 °C for 10 min in an electric oven. Next, the cleaned FTO substrates were treated using an UV ozone cleaner for 10 min. A buffer layer solution was prepared using 0.5 ml titanium butoxide (reagent 97%, Aldrich), 9 ml 2-methoxyethanol and 0.18 ml monoethanolamine as the precursor, solvent and stabilizer, respectively. The buffer layer solution was stirred at 250 rpm for 3 hours. The solution was dispersed using a spin coater (JD-Tech, JSP4D) on the FTO substrates at 500 rpm for 5 s and at 4000 rpm for 30 s. The substrate coated with the buffer-solution was dried at 115 °C for 10 min in an electric oven. The spin-coating and drying processes were repeated twice. Then, the FTO substrates were annealed in air at 550 °C for 2 hours. TiO_2 nanorods were grown on the TiO_2 buffered FTO substrates using a hydrothermal method. To prepare the precursor solution, the precursors were each dissolved separately in 10 ml of DI water and 10 ml of HCl (37%) in a Teflon container. To study the effects of precursor concentration, each titanium precursor was prepared as solutions with concentrations of 0.015 M, 0.03 M, 0.06 M, 0.09 M, 0.15 M, 0.3 M and 0.6 M. Then, each solution was placed in a Teflon container and put into steel vessels, which were sealed and heated in an oven at 180 °C for 4 hours. The vessels were then cooled to room temperature for 2 hours, and the samples were removed from the vessels, rinsed in distilled water and dried by filtered air. The samples were annealed in air at 500 °C for 6 hours. Field emission scanning electron microscopy (FE-SEM) and atomic force microscopy (AFM) were used to characterize the morphology of the nanorods, X-ray diffraction (XRD) was used to detect the structural properties of the nanorods, UV-visual spectroscopy was used to measure the optical properties, and a three-electrode potentiostat was used to measure the photoelectrochemical properties. The substrate coated with the aligned TiO_2 nanorod grown with various titanium precursor concentrations was used as the working electrode, graphite was used as the counter electrode, and a saturated calomel electrode (SCE) was used as the standard electrode. A voltammetric sweep was performed from −1.0 V to 1.5 V. A 1 M KOH aqueous solution (pH = 13.5) was used as the electrolyte. A 300-W Xenon lamp with 1-sun illumination (AM 1.5 filter, 100 mW/cm^2) was employed as the light source.

3. RESULTS AND DISCUSSION

Figure 1 shows the top view and cross-sectional SEM images of the TiO_2 nanostructures grown on FTO substrates with titanium precursor concentrations of 0.015 M, 0.03 M, 0.06 M, 0.09 M, 0.15 M, 0.3 M and 0.6 M. The TiO_2 nanorods began to appear at a precursor concentration of 0.015 M. A low density of TiO_2 nanorods grew from the 0.03 M and 0.06 M samples and grew irregularly and diagonally. This is because the low precursor concentration led to fewer nucleation sites for TiO_2 nanorod growth.[24] The nanorods grown from the 0.09 M and 0.15 M solutions exhibited better vertical alignment, and denser TiO_2 nanorod arrays were produced by the 0.3 M and 0.6 M solutions. In addition, coalesced shapes could also be observed from the 0.3 M and 0.6 M samples. It is generally known that the number of nucleation sites depends on the precursor concentration. Therefore, a larger number of nucleation sites

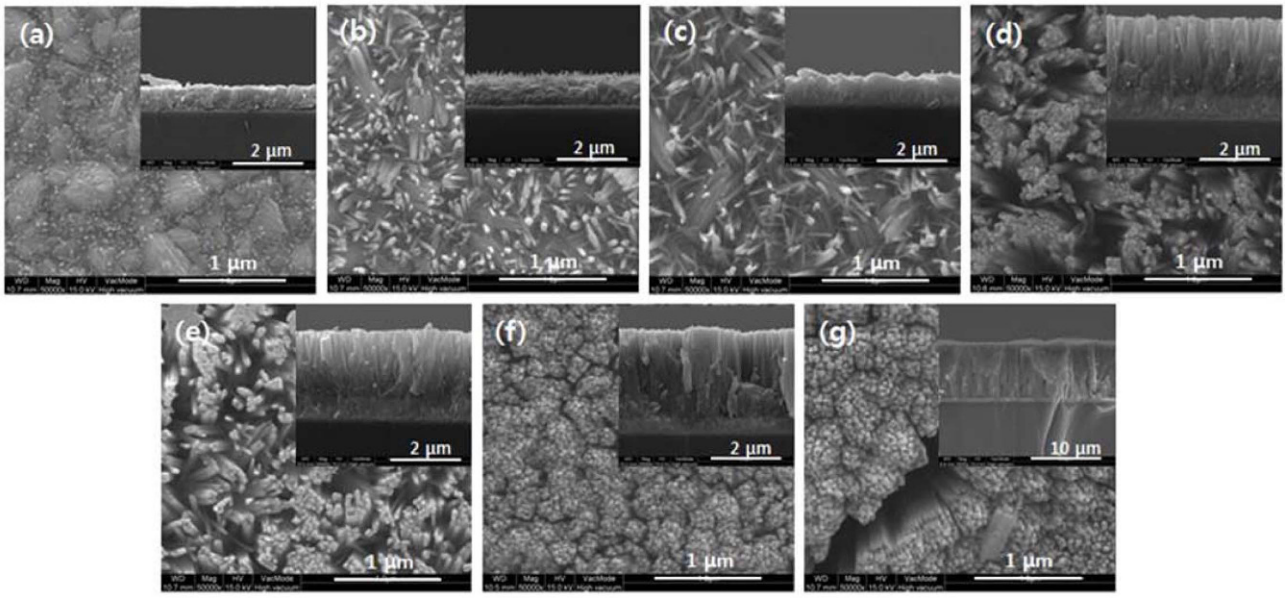

Fig. 1. Top view and cross-sectional SEM images of TiO_2 nanorods grown from solutions with precursor concentrations of (a) 0.015 M, (b) 0.03 M, (c) 0.06 M, (d) 0.09 M, (e) 0.15 M, (f) 0.3 M, and (g) 0.6 M.

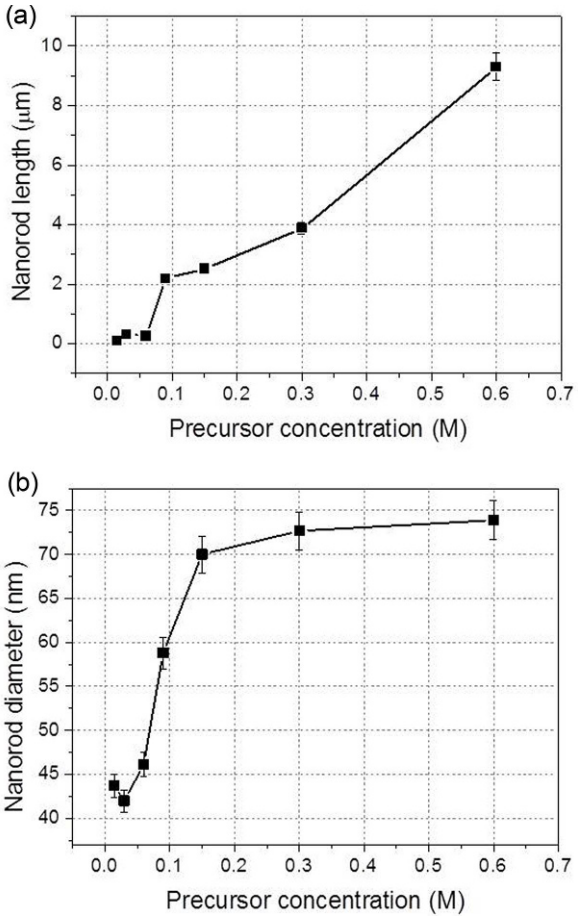

Fig. 2. (a) The length of TiO_2 nanorods and (b) the diameter of TiO_2 nanorods as a function of the precursor concentration.

can lead to denser coverage of nanorods and consequently nanorod coalescence at high precursor concentration.[32] Figure 2(a) and (b) show the length and diameter of the TiO_2 nanorods grown on the FTO substrate at the series of precursor concentrations. The length and diameter of the TiO_2 nanorods increased with increasing precursor concentration. The length and diameter increased significantly when the precursor concentration exceeded 0.09 M. Generally, the diameter and length of nanorods increase as the precursor concentration increases since the crystal growth rate at the liquid-solid interface is proportional to the concentration.[33]

The AFM surface image and roughness of the TiO_2 nanorods at various precursor concentrations are shown in Fig. 3. As the precursor concentration increases up to 0.09 M, the roughness increases, but the roughness decreased for precursor concentrations above 0.15 M, possibly due to the coalescence at high concentration, as discussed for Fig. 1. Figure 4(a)-(g) show the AFM cross-sectional images of TiO_2 nanorods grown at the series of precursor concentrations, and the surface areas of the TiO_2 nanorods are shown in Fig. 4(h). The surface areas were obtained using AFM top view images. *S*imilar to the results of roughness in Fig. 3(h), the surface area increased with increasing precursor concentration up to a concentration of 0.09 M and then decreased at concentrations greater than 0.09 M, which is also an effect of coalescence.

Figure 5 shows the transmittance for samples grown at various precursor concentrations ranging from 0.015 M to 0.6 M. As the nanorod length increases, the transmittance

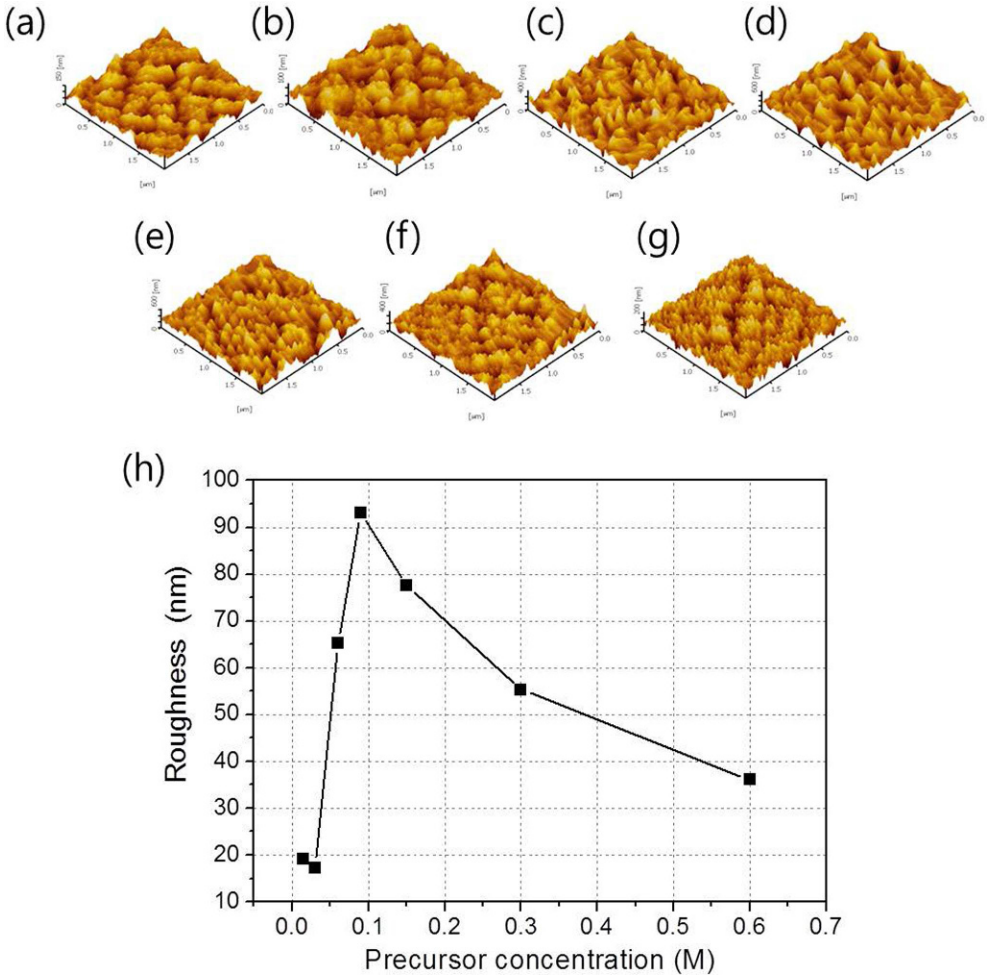

Fig. 3. AFM 3-D images of TiO_2 nanorods grown from precursor solutions with concentrations of (a) 0.015 M, (b) 0.03 M, (c) 0.06 M, (d) 0.09 M, (e) 0.15 M, (f) 0.3 M, and (g) 0.6 M. (h) Roughness values as a function of the precursor concentration.

value decreases in this study. The transmittance property significantly changed at a concentration of approximately 0.09 M. It is known that the length of the TiO_2 nanorods has a significant impact on the transmittance value. In general, samples with fewer or shorter nanorods have a higher transmittance since light can be transmitted more easily through the thin sample. Recently, Meng *et al*. reported that transmittance decreased as the TiO_2 nanorod length increased.[34]

Figure 6(a) presents the XRD patterns of the samples synthesized using various titanium precursor concentrations. The peaks in the XRD patterns at 2θ = 26°, 37.5°, 52°, 62° and 66° are from tin dioxide (SnO_2) in the FTO substrate (ICSD Card No. 98-005-6672), and the peak at 2θ = 62.87° is identified as the (002) plane of the tetragonal rutile phase of TiO_2 (ICSD Card No. 98-008-5493). The (002) peak intensities are shown in Fig. 6(b). In general, (002) peak intensity indicates the degree of orientation. That is, the higher the intensity of the (002) peak, the more the nanorods are oriented perpendicular to the substrate.[35,36] The (002) peak intensities of the 0.015 M, 0.03 M and 0.06 M samples are relatively insignificant because the nanorods did not grow perpendicular to the substrate in those cases. The (002) peak intensities of the 0.09 M and 0.15 M samples gradually increase due to the growth of the nanorods perpendicular to the substrate, as shown in Fig. 1. The (002) peak intensity of the samples that used the highest concentration of precursors, 0.3 M and 0.6 M, significantly increased. That is, the most oriented nanorod growth could be found for the samples grown at the highest precursor concentration in this study.

The photoelectrochemical properties of the samples grown at various precursor concentrations are presented in Fig. 7. In Fig. 7(a), the photocurrent densities are shown under illumination and dark conditions with an applied potential of −1.0 V to 1.5 V (vs. SCE). The open-circuit voltage (V_{oc}) appears at −0.79 V in all samples. Figure 7(b) presents the photocurrent density of samples with an applied potential of

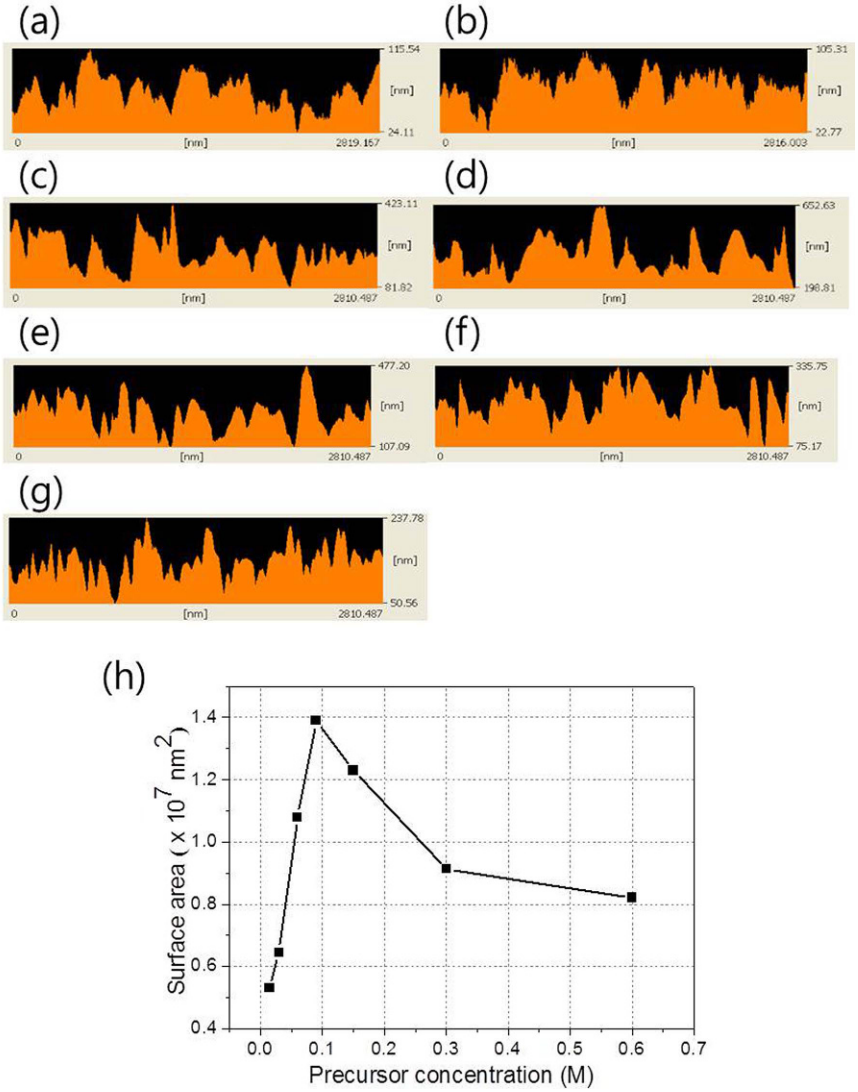

Fig. 4. AFM images of TiO_2 nanorods grown from precursor solutions with concentrations of (a) 0.015 M, (b) 0.03 M, (c) 0.06 M, (d) 0.09 M, (e) 0.15 M, (f) 0.3 M, and (g) 0.6 M. (h) Surface area values as a function of the precursor concentration.

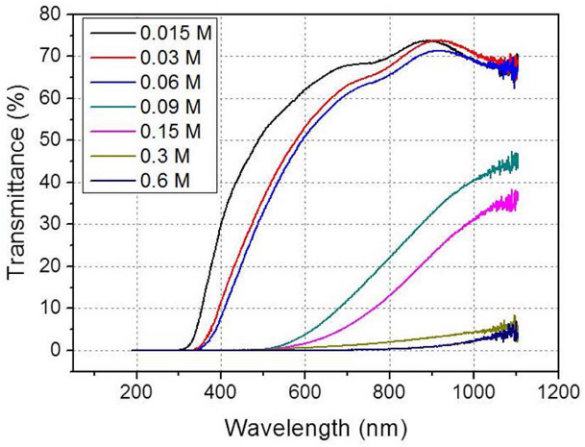

Fig. 5. Transmittance of TiO_2 nanorods as a function of the precursor concentration.

1.0 V (vs. SCE). The photocurrent density increased for increasing precursor concentrations up to 0.09 M, then decreased for precursor concentrations above 0.09 M. The maximum photocurrent density is 0.733 mA/cm² from the 0.09 M sample.

Figure 8 shows the relationship between the various properties discussed above such as the morphological, structural properties and the photoelectrochemical properties. Figure 8(a) shows the relationship between the nanorod length and the photocurrent density value. Although the nanorod length increased continuously as the precursor concentration increased in this study, the photocurrent density value increased for concentrations up to 0.09 M and then decreased for concentrations greater than 0.09 M. It was generally known that increasing the nanorod length could improve the photoelectrochemical property.[37-39] 1-D nanorods can

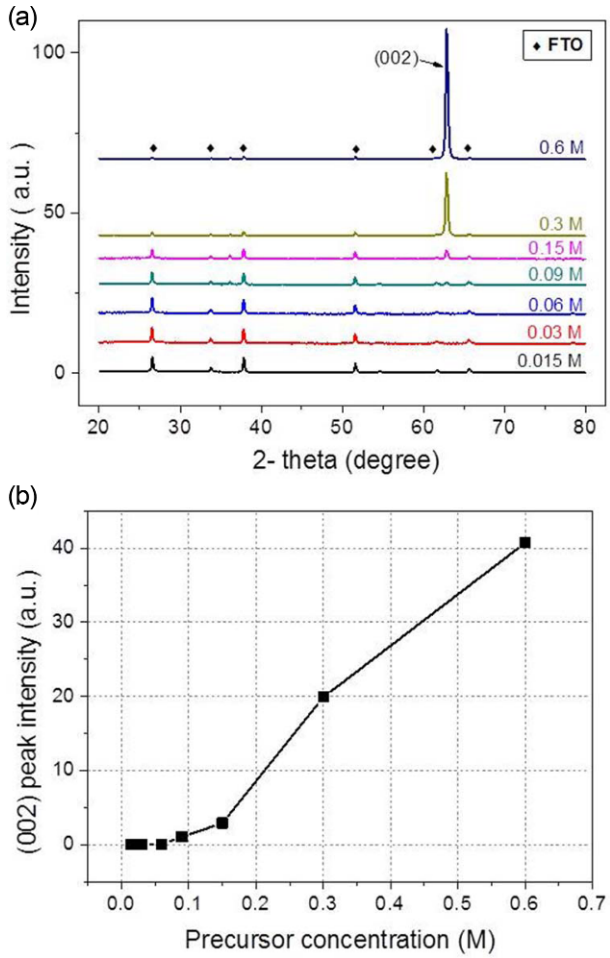

Fig. 6. XRD result for the TiO_2 nanorods on FTO substrate as a function of the precursor concentrations: 0.015 M, 0.03 M, 0.06 M, 0.09 M, 0.15 M, and 0.3 M. (a) XRD spectra, (b) (002) peak intensity.

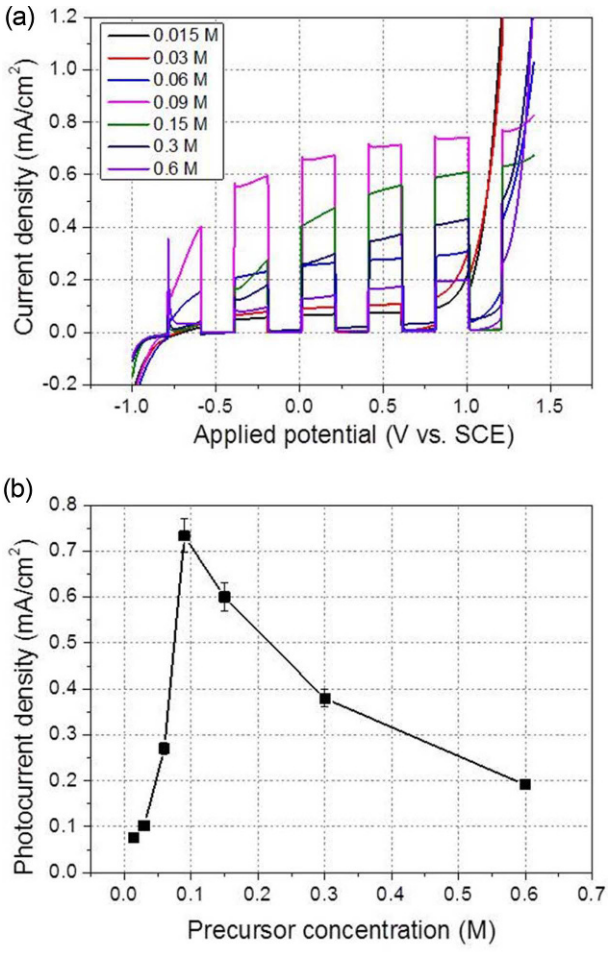

Fig. 7. PEC performance for TiO_2 nanorods on FTO substrate as a function of the precursor concentrations: (a) plots of photocurrent density vs. SCE, (b) photocurrent density at 1.0 V.

minimize electron-hole pair recombination because the diffusion length at the 1-D TiO_2 photoelectrode/electrolyte interface can decrease.[40] Therefore, nanorods can transport more holes into the electrolyte as the nanorod length increases.[41] However, excessive nanorods length can have a negative impact on the photoelectrochemical property.[42] Feng *et al.* reported that TiO_2 nanorods having excessive length due to excessively long growth time can fuse at their roots due to an increase in the lateral dimension of the base of the nanorods.[35] The nanorods are then coalesced and the photoelectrochemical properties can be reduced.[43] With excessive nanorod length, carrier recombination can occur more easily before the minority carrier, the hole, escapes from the TiO_2 nanorods into the electrolyte, which can also degrade the photoelectrochemical property. Thus, these previous reports may explain our finding that the photocurrent density value increased for precursor concentrations up to 0.09 M and then decreased for concentrations above 0.09 M.

Figure 8(b) presents the relation between the surface areas of TiO_2 nanorod and the photocurrent density values for various concentration samples. As the precursor concentration increases up to 0.09 M, both the surface area of TiO_2 nanorod and the photocurrent density value increased. The increase in the surface area means an increased contact area between the electrolyte and TiO_2 nanorods, leading to the increase of the photocurrent density values. This is because the minority carriers, the holes, can escape from the TiO_2 nanorods into the electrolyte more easily with a higher contact area. However, as mentioned in Fig. 8(a), nanorod having excessive length coalesce with each other at the higher precursor concentrations. Therefore, the surface area for samples with excessive nanorod length significantly decreases[42] and photocurrent density also decreases.

Figure 8(c) shows the (002) XRD peak intensity and photocurrent density values for the various concentration samples. (002) XRD peak intensity increases as the precursor concentration increases and the photocurrent density value increases up to a precursor concentration of

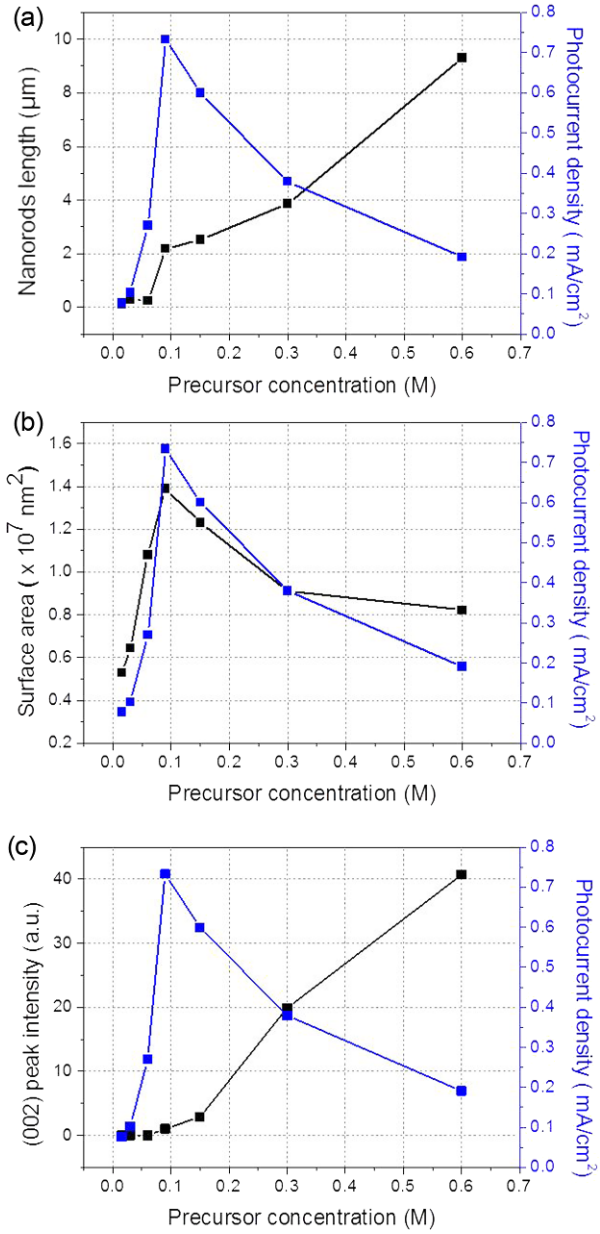

Fig. 8. (a) Nanorod length and photocurrent density, (b) surface area and photocurrent density, and (c) (002) peak intensity and photocurrent density as a function of the precursor concentration.

0.09 M and then decreases. In general, it is known that the photocurrent density value also increases with (002) XRD peak intensity which indicates growth oriented perpendicular to the substrate. Previous studies have reported that as the (002) XRD peak intensity of TiO_2 nanorods grown by the hydrothermal method increased, the photoelectrochemical property improved.[28,44] However, the photocurrent density value does not show a similar trend with the (002) peak intensity in this study. The sample with the highest photocurrent density has a low (002) peak intensity, as shown in Fig. 8(c). This result could be proof that the influences of the nanorod length and surface area are greater than that of the (002) peak intensity.

Additionally, the transmittance value decreases continuously with increasing precursor concentration, as discussed for Fig. 5. That is, the transmittance value decreases as the nanorod length increases since longer nanorod can absorb more photons. The photocurrent density has the highest value at a concentration of 0.09 M and then decreases at higher concentrations. Generally, sample with low transmittance can have a high photocurrent density because they absorb more photons. However, in this study, the photocurrent density value decreases even though the transmittance value decreases for the samples grown with precursor concentrations greater than 0.09 M. A previous study reported that when the transmittance decreases below a certain threshold value, the incident light intensity onto the surface of TiO_2 is reduced, resulting in a decrease of the number of excited electrons and leading to the decline of the photoelectrochemical property.[41] Thus, the previously reported results may explain our results.

4. CONCLUSIONS

In this study, the morphological, optical, structural and photoelectrochemical properties of TiO_2 nanorods grown with various precursor concentrations by the hydrothermal method were studied, and the relationship of each property to the precursor concentration was systematically analyzed. The TiO_2 nanorods grown at relatively low concentrations were short and not oriented perpendicular to the substrate, which resulted in degraded photoelectrochemical properties. In addition, when the precursor concentration is excessively increased, the photoelectrochemical property deteriorates due to coalescence of the TiO_2 nanorods. From this study, we found that the TiO_2 nanorod length, diameter and (002) peak intensity affected the photoelectrochemical property. Additionally, the TiO_2 nanorod surface area in contact with the electrolyte also had a strong influence on the photoelectrochemical property. Therefore, the morphological, optical, structural and photoelectrochemical properties are dependent on the precursor concentration, and the highest photocurrent density, 0.733 mA/cm^2 (at 1.0 V vs. SCE), was obtained from the 0.09 M sample.

ACKNOWLEDGEMENTS

This research was supported by Basic Science Research Program through the National Research Foundation of Korea (NRF) funded by the Ministry of Education (NRF-2016R1D1A3B01008959).

REFERENCES

1. T. Bak, J. Nowotny, M. Rekas, and C. C. Sorrell, *Int. J.*

Hydrogen Energ. **36**, 991 (2002).
2. J. Lee, Y. Yi, and S. Uhm, *J. Korean Ind. Eng. Chem.* **19**, 357 (2008).
3. M. Gratzel, *Nature* **414**, 338 (2001).
4. J. Nowotny, C. C. Sorrell, L. R. Sheppard, and T. Bak, *Int. J. Hydrogen Energ*. **30**, 521 (2005).
5. J. Zhu and M. Zach, *Curr. Opin. Colloid Interface Sci.* **14**, 260 (2009).
6. J. Cui and U. J. Gibson, *J. Phys. Chem.* **114**, 6408 (2010).
7. I. S. Cho, Z. Chen, A. J. Forman, D. R. Kim, P. M. Rao, T. F. Jaramillo, and X. Zheng, *Nano Lett*. **11**, 4978 (2011).
8. W. Wang, W. Zhang, S. Meng, L. Jia, M. Tan, C. Hao, Y. Liang, J. Wang, and B. Zou, *Electron. Mater. Lett*. **12**, 753 (2016).
9. Y. S. Chaudhary, A. Agrawal, R. Shrivastav, V. R. Satsangi, and S. Dass, *Int. J. Hydrogen Energ.* **29**, 131 (2004).
10. Y. C. Pu, G. Wang, K. D. Chang, Y. Ling, Y. K. Lin, B. C. Fitzmorris, C. M. Liu, X. Lu, Y. Tong, J. Z. Zhang, Y. J. Hsu, and Y. Li, *Nano Lett.* **13**, 3817 (2013).
11. A. N. Banerjee, *Nanotechnol. Sci. Appl.* **4**, 35 (2011).
12. J. H. Bang and P. V. Kamat, *Adv. Funct. Mater*. **20**, 1970 (2010).
13. A. M. More, T. P. Gunjakar, C. E. Lokhande, and O. S. Joo, *Appl. Surf. Sci.* **255**, 2682 (2008).
14. G. K. Mor, K. Shankar, M. Paulose, O. K. Varghese, and C. A. Grimes, *Nano Lett.* **6**, 215 (2006).
15. J. C. Lee, T. G. Kim, W. Lee, S. H. Han, and Y. M. Sung, *Cryst. Growth Des.* **9**, 4519 (2009).
16. N. Liu, X. Chen, J. Zhang, and J. W. Schwank, *Catal. Today* **225**, 34 (2014).
17. T. D. N. Phan, H. DinhPham, T. V. Cuong, E. J. Kim, S. Kim, and E. W. Shin, *J. Cryst. Growth* **312**, 79 (2009).
18. D. S. Kim and S. Y. Kwak, *Appl. Catal. A: Gen.* **323**, 110 (2007).
19. K. H. Tam, A. B. Djurisic, C. M. N. Chan, Y. Y. Xi, C. W. Tse, Y. H. Leung, W. K. Chan, F. C. C. Leung, and D. W. T. Au, *Thin Solid Films* **516**, 6167 (2008).
20. T. Sahoo, S. K. Tripathy, Y. T. Yu, H. K. Ahn, D. C. Shin, and I. H. Lee, *Mater. Res. Bull*. **4**, 2060 (2008).
21. S. Li, S. Zhou, H. Liu, Y. Hang, C. Xia, J. Xu, S. Gu, and R. Zhang, *Mater. Lett.* **61**, 30 (2007).
22. M. N. R. Ashfold, R. P. Doherty, N. G. N. Angwafor, D. J. Riley, and Y. Sun, *Thin Solid Films* **515**, 8679 (2007).
23. M. Guo, P. Diao, and S. Cai, *J. Solid State Chem.* **178**, 1864 (2005).
24. B. Liu and E. S. Aydil, *Chinese Phys. B* **23**, 048104 (2014).
25. Y. Zhao, W. Yang, Y. Zhou, Y. Chen, Y. Yang, J. Xu, and Y. Jiang, *Electron. Mater. Lett*. **12**, 779 (2016).
26. H. B. Oh, H. H. Ryu, and W. J. Lee, *J. Alloy. Compd.* **620**, 55 (2015).
27. X. Zhao, J. Y. Lee, C. R. Kim, J. H. Heo, C. M. Shin, J. Y. Leem, H. H. Ryu, J. H. Chang, H. C. Lee, W. G. Jung, C. S. Son, B. C. Shin, W. J. Lee, S. T. Tan, J. L. Zhao, and X. W. Sun, *Physica E* **41**, 121423 (2009).
28. M. Iraj, F. D. Nayeri, E. A. Soleimani, and K. Narimani, *J. Alloy. Compd.* **659**, 44 (2016).
29. M. Rajabi, S. Shogh, and A. Irajizad, *J. Lumin.* **157**, 235 (2015).
30. Y. L. M. Guo, M. Zhang, and X. Wang, *Mater. Res. Bull.* **44**, 1232 (2009).
31. H. E. Wang, Z. Chen, Y. H. Leung, C. Luan, C. Liu, Y. Tang, C. Yan, W. Zhang, J. A. Zapien, I. Bello, and S. T. Lee, *Appl. Phys. Lett.* **96**, 263104 (2010).
32. Y. H. Liou, S. L. Lo, W. H. Kuan, C. J. Lin, and S. C. Weng, *Water Res.* **40**, 2485 (2006).
33. Z. Gui, X. Wang, J. Liu, S. Yan, Y. Ding, Z. Wang, and Y. Hu, *J. Solid State Chem.* **179**, 1984 (2006).
34. L. Meng, H. Chen, C. Li, and M. P. Santos, *Thin Solid Films* **577**, 103 (2015).
35. X. J. Feng, K. Shankar, O. K. Varghese, M. Paulose, T. J. Latempa, and C. A. Grimes, *Nano Lett*. **8**, 3781 (2008).
36. H. Chen, W. Fu, H. Yang, P. Sun, Y. Zhang, L. Wang, W. Zhaoa, X. Zhou, H. Zhao, Q. Jing, X. Qi, and Y. Li, *Electrochim. Acta* **56**, 919 (2010).
37. S. A. Vanalakar, S. S. Mali, R. C. Pawar, N. L. Tarwal, A. V. Moholkar, J. H. Kim, and P. S. Patil, *J. Appl. Phys.* **112**, 044302 (2012).
38. J. Bian, C. Huang, L. Wang, T. Hung, W. A. Daoud, and R. Zhang, *ACS Appl. Mater. Inter.* **6**, 4883 (2014).
39. Y. J. Hwang, C. Hahn, B. Liu, and P. Yang, *ACS Nano* **6**, 5060 (2012).
40. X. Zhao, W. Luo, J. Feng, M. Li, Z. Li, and T. Yu, *Adv. Energy Mater.* **4**, 1601785 (2014).
41. X. Zheng, S. Shen, F. Ren, G. Cai, Z. Xing, Y. Liu, D. Liu, G. Zhang, X. Xiao, W. Wu, and C. Jiang, *Int. J. Hydrogen Energ.* **40**, 5034 (2015).
42. T. Hamamura, J. T. Dy, K. Tamaki, J. Nakazaki, S. Uchida, T. Kuboa, and H. Segawa, *Chem. Phys*. **16**, 4551 (2014).
43. Z. Zhou, J. Fan, X. Wang, W. Zhou, Z. Du, and S. Wu, *ACS Appl. Mater. Inter.* **3**, 4349 (2011).
44. C. Y. Kim, H.-B. Oh, H. Ryu, J. Yun, and W.-J. Lee, *J. Vac. Sci. Technol. A*, **32**, 051505 (2014).